

Shear Flow Rheological Properties, Fiber Damage, and Mastication Characteristics of Aramid-, Glass-, and Cellulose-Fiber-Reinforced Polystyrene Melts

LECH CZARNECKI* and JAMES L. WHITE, *Polymer Engineering, University of Tennessee, Knoxville, Tennessee 37916*

Synopsis

An experimental study of the viscosity and principal normal stress difference of a polystyrene melt filled with aramid (Kevlar), glass, and cellulose fibers is reported. The influence of loading level and mastication on the rheological properties is discussed. The effects of mixing and mastication on fiber damage are considered. Glass fibers break down rapidly to very small aspect ratios, while aramid shows a "kinked" structure, with kinks occurring every 100 μm . A mechanism is proposed for fiber breakage based on buckling during rotation in shear flow. It is found that addition of fibers increases the viscosity in the same manner as a reduction in temperature, and data may be superposed by reduced plotting. This indicates that the viscosity increase is due solely to enhanced viscous dissipation in the matrix and not to interparticle forces as is the case with smaller particles. The principal normal stress difference increases at fixed shear stress with fiber loading. The extent of increase depends upon fiber loading, aspect ratio, and modulus.

INTRODUCTION

The mechanics and properties of composites have received considerable attention in the literature.¹⁻⁶ Few studies of the rheological properties of fiber-filled polymer melts have appeared,⁷⁻¹⁰ and these deal solely with glass-fiber-filled melts. With the exception of the study of Chan, White, and Oyanagi,⁹ all of these investigations are limited to high shear rate extrusion-based shear viscosity measurements. These researchers have established that the shear viscosity of suspensions of glass fibers is independent of the type of measurement. Chan et al.⁹ determined shear flow normal stresses, which they found to be enhanced by the presence of fibers, as well as the elongational viscosity, which was found to be large at low deformation rates and then to decrease with increasing rates of elongation. Extrudate swell has been found to be suppressed by the presence of fibers,^{8,9} while die entrance pressure losses were significantly increased.⁹ Recently, Wu¹⁰ has investigated fiber migration during flow of glass-fiber-reinforced melts.

The investigations above represent a first generation of investigations mapping out the general characteristics of polymer melts reinforced with fibers. There was little consideration of the influence of (1) fiber type and properties; (2) diameter, aspect ratio, and length distribution, or (3) the character of the induced fiber damage. A first study of fiber breakage in mixing has been reported by O'Connor¹¹ but without detailed consideration of either distinctive differences

* Present address: Department of Civil Engineering, Warsaw Technical University, 00637-Warsaw, Poland.

in types of fiber damage or influence on rheological properties. O'Connor does contrast cellulose, glass, aramid (Kevlar), and nylon fibers. Some considerations of glass fiber length distributions and the effect of aspect ratio on the viscosity of silicone oil is given by Maschmeyer and Hill.¹² Effects of processing conditions on properties of fiber-reinforced products are discussed by Goettler,^{13,14} Zielinski,³ Zakrzewski,⁴ Kohman,⁵ Moghe,¹⁵ and O'Connor.¹¹ The results of Goettler appear to primarily represent the influence of fiber orientation. O'Connor shows the effect of fiber damage in deterioration of properties.

In this paper we turn our attention to this series of problems. We consider the differing characteristics of glass, aramid (Kevlar), and cellulose fibers and their influence on rheological properties. The damage of the fibers during mixing and in processing is investigated, and its influence on rheological properties is measured. This paper continues our ongoing investigations of the rheological properties of particle-reinforced polymer melts.^{9,16-20}

EXPERIMENTAL

Materials

The systems investigated in this study were compounds of polystyrene with glass, organic aromatic polyamide (aramid, Kevlar), and cellulose fibers. The characteristics of these fibers are summarized in Table I. The glass-fiber-reinforced polymer was supplied by the Fiberfil Division of Dart Industries and was the same system studied by Chan et al.⁹ The cellulose fibers were Westvaco Pinnacle pulp, and the aramid was Kevlar 29 of du Pont. Table II summarizes the volume and weight fractions studied in the different melts.

Mixing

The aramid and cellulose fibers were dispersed using a combination of a two-roll mill and a $\frac{3}{4}$ -in. Brabender screw extruder. The systems were first massed in the laboratory mill having 3×7 -in. rolls for an average period of 45 min at 160°C and then extruded with the screw extruder at 180°C with a screw speed of 30 rpm.

Mastication

We sought to determine the influence of prolonged mastication of the composite melt on the fiber length distribution. The mastication was carried out for periods of 30 min and 1 hr, and in the case of the aramid composite, for also 90 min, on the roll mill at a temperature of 150°C.

TABLE I
Fiber Characteristics

Characteristics	Glass ^{11,21}	Fiber Kevlar ^{11,21}	Cellulose ¹¹
Density	2.5	1.44	1.5
Diameter, μm	12.7	12.2	12
Tensile modulus, $\times 10^{-9}$ Pa	69-74	82-84	20
Tensile strength, $\times 10^{-8}$ Pa	15.35	28-30	5.2

TABLE II
Fiber Loadings Investigated^a

Fiber	Weight w	Loadings, %	
		Volume ϕ_{20} (20°C)	Volume ϕ_{180} (180°C)
Glass	0	0	0
	20	9.5	8.6
	40	22	20.2
Aramid (Kevlar 29)	0	0	0
	1.3	1	0.9
	6.6	5	4.4
	13.0	10	9.1
Cellulose	25.3	20	18.4
	0	0	0
	7.1	5	4.8
	27.2	20	19.6

$$^a \phi = \frac{w_F/\rho_F}{(w_F/\rho_F) + ([1 - w_F]/\rho_P)}, \text{ where } F = \text{fiber, } P = \text{polymer.}$$

Investigation of Fiber Character

Before and after mixing, the character of the aramid and cellulose fibers was investigated by optical and scanning electron microscopy (SEM). The polystyrene was dissolved away from the compounds. We also investigated the glass fibers in the samples supplied by Fiberfil. In addition, the masticated cellulose and aramid fibers were similarly studied.

The optical microscopy studies used an Ortholux microscope (model 72748 Leitz Wetzlar).

The SEM investigations utilized an AMR model 900 high-resolution scanning electron microscope (Advanced Metals Research Corp., Burlington, MA). A gold-palladium alloy was used on the fibers to eliminate charging in the electron beam.

Rheological Measurements

Measurements of the steady-state shear stress $\sigma_{12}(\dot{\gamma})$ and principal normal stress difference $N_1(\dot{\gamma})$ ($\sigma_{11} - \sigma_{22}$) were made on a Rheometrics mechanical spectrometer over a range of shear rates. The shear stress was measured through the torque T , and the principal normal stress difference through the thrust F using the expressions²²

$$\sigma_{12} = \frac{3T}{2\pi R^3} \quad N_1 = \frac{2F}{\pi R^2} \quad (1)$$

where R is the cone radius. The shear rate in the gap is given by

$$\dot{\gamma} = \frac{\Omega}{\alpha} \quad (2)$$

where Ω is the angular velocity and α is the cone angle. A cone diameter of 25 cm with an angle of 0.1 rad was used in these studies.

FIBER CHARACTER AND LENGTH DISTRIBUTION IN COMPOSITES

Results

In Figures 1 and 2 we summarize SEM photomicrographs of the initial cellulose and aramid fibers. In Figure 3 we show photomicrographs of the glass fibers in the compounds as received from Fiberfil after the polystyrene has been removed. In Figures 4 and 5 we show the cellulose and Kevlar fibers in the initial compounds.

These fiber-polymer composites were also subjected to intensive mill mastication as described in the previous section. SEM photomicrographs showing the fibers removed from masticated samples are illustrated in Figures 6 through 8. Optical photomicrographs of aramid fibers are shown in Figure 9.

From Figures 1 through 9, we can see the development of damage of the fibers. The characteristics of the fibers are different. The glass fibers apparently undergo a "clean" break. This is not found in the Kevlar or cellulose fibers. The aramid fibers after mixing and further mastication exhibit a series of "bends" or "kinks" which eventually result in breakage. The cellulose fibers exhibit no substantial change during processing. They appear very much like cotton fibers^{23,24} and seem self-buckled into a helical structure, probably because of removal of internal moisture.

The extent of breakage in processing and mastication is most rapid and severe in the glass fibers and apparently least in cellulose. The rate of breakdown seems intermediate in the aramid fibers.

Discussion

Fiber breakage results in changes not only in average length but in the distribution of lengths. For the case of the glass fibers, where the breakage is clean,

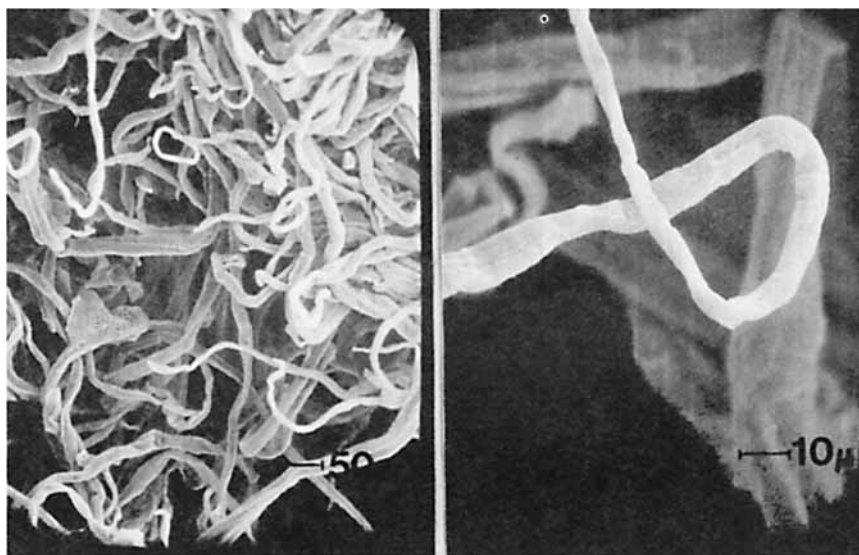


Fig. 1. SEM photomicrographs of virgin cellulose fibers.

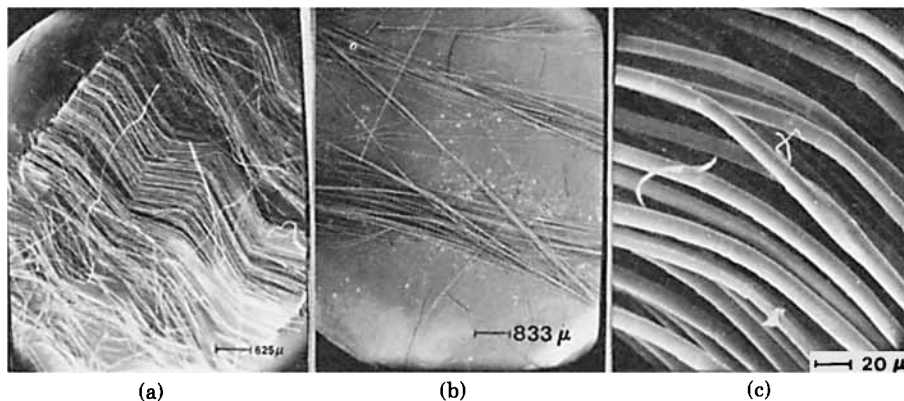


Fig. 2. SEM photomicrographs of virgin Kevlar 29 fibers. Initial length l_0 (a) 635 μm ; (b) 127 μm . (c) Diameter $D = 12.2 \mu\text{m}$.

the situation is the clearest. Figure 10 shows length distributions of glass fibers based upon 100 fibers in the composite as received from Fiberfil and the distributions of lengths after periods of mastication of 30 and 60 min at 150°C. It can be seen that not only is the average length reduced but the distribution may change. To check this need, we need to look in more detail at the specifications of the distribution.

We may represent the distribution of fiber lengths in terms of moments of the distribution much in the way a polymer chemist describes molecular weight distribution.²⁵ Specifically, we may define number-, weight-, and z -average lengths through

$$L_n = \frac{\sum N_i L_i}{\sum N_i} \quad (3a)$$

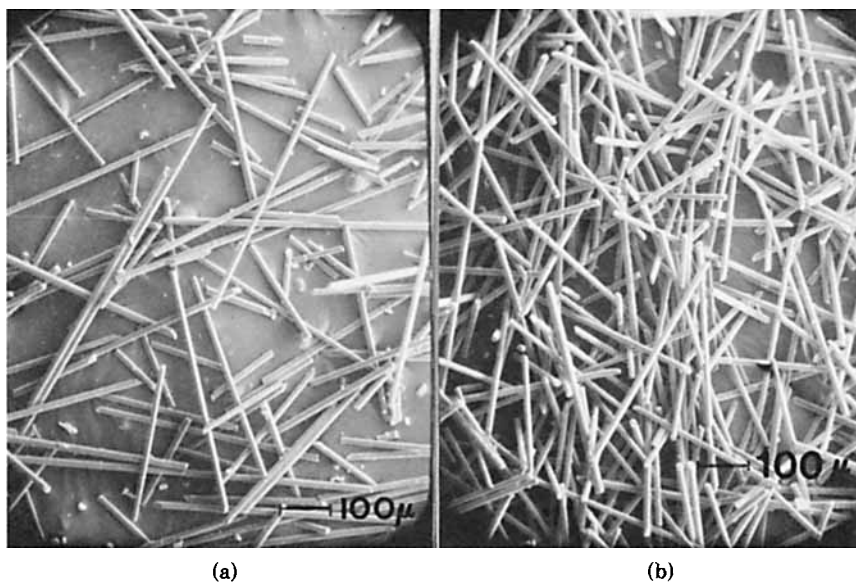


Fig. 3. SEM photomicrographs of glass fibers in the initial compounds: (a) $\phi = 9.5\%$, (b) and $\phi = 22\%$.

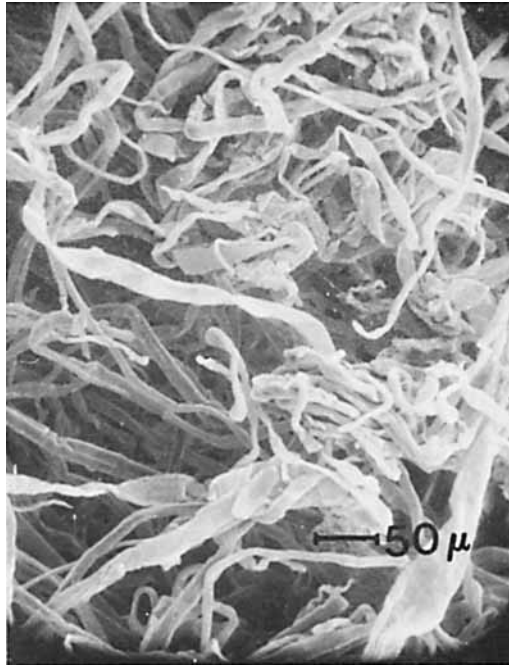


Fig. 4. SEM photomicrographs of cellulose fibers in the initial compounds.

$$L_w = \frac{\sum N_i L_i^2}{\sum N_i L_i} \quad (3b)$$

$$L_z = \frac{\sum N_i L_i^3}{\sum N_i L_i^2} \quad (3c)$$

We summarize values of L_n , L_w , and L_z and their ratios for the initial and masticated fiber samples in Table III for glass and in Table IV and Figure 11 for

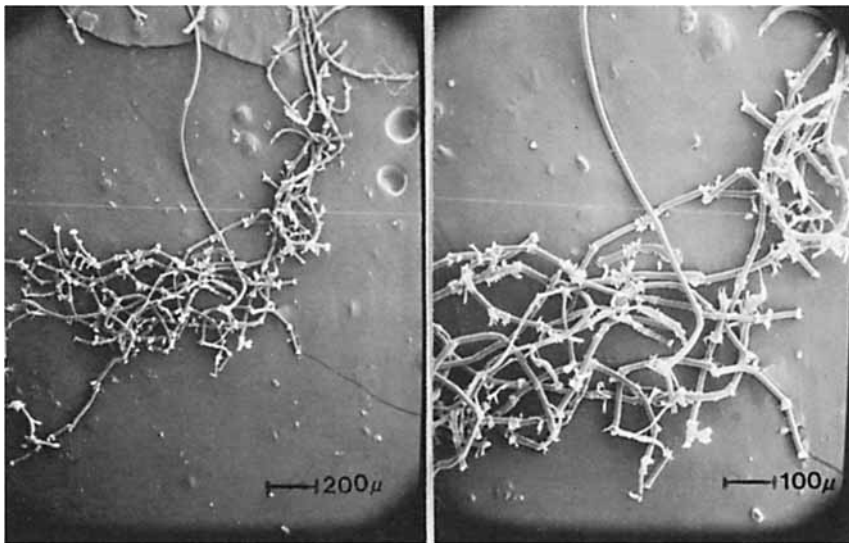


Fig. 5. SEM photomicrographs of Kevlar fibers in the initial compounds.

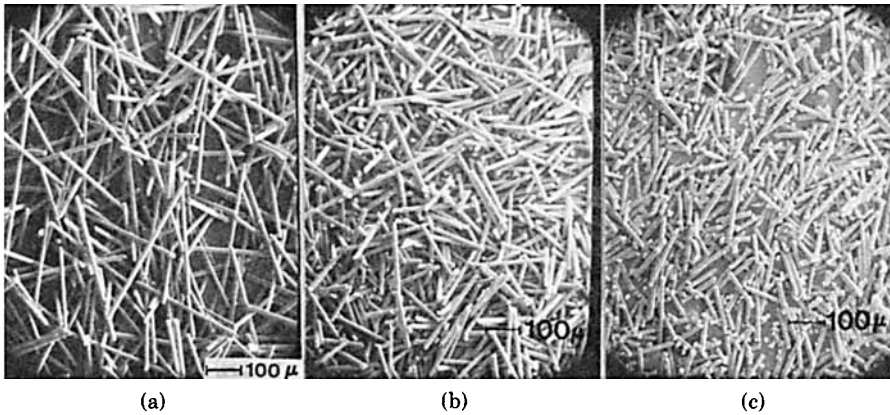


Fig. 6. SEM photomicrographs of glass fibers: (a) initial compound; (b) 30 min masticated; (c) and 60 min masticated.

Kevlar fibers. The value of L_w/L_n , the polydispersity index, remains about the same during mixing and mastication of the glass.

We have also attempted to represent the mastication breakdown of the aramid and cellulose fiber samples. If we neglect kink effects (see Figs. 5 and 8) and only include clean breaks, we obtain for Kevlar the results shown in Table IV. Moghe¹⁵ shows a similar picture of “kinked” aramid fibers. The individual kink “quasi-break” morphology shows some similarity to SEM photomicrographs taken by Konopasek and Hearle²⁶ (their Fig. 6), but there are differences. If we consider the distance between kinks, we find that this distance is a constant

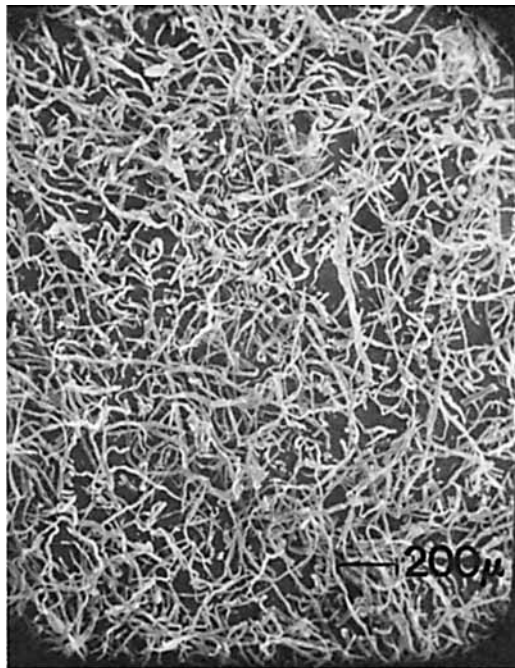


Fig. 7. SEM photomicrographs of roll mill-masticated cellulose fibers.

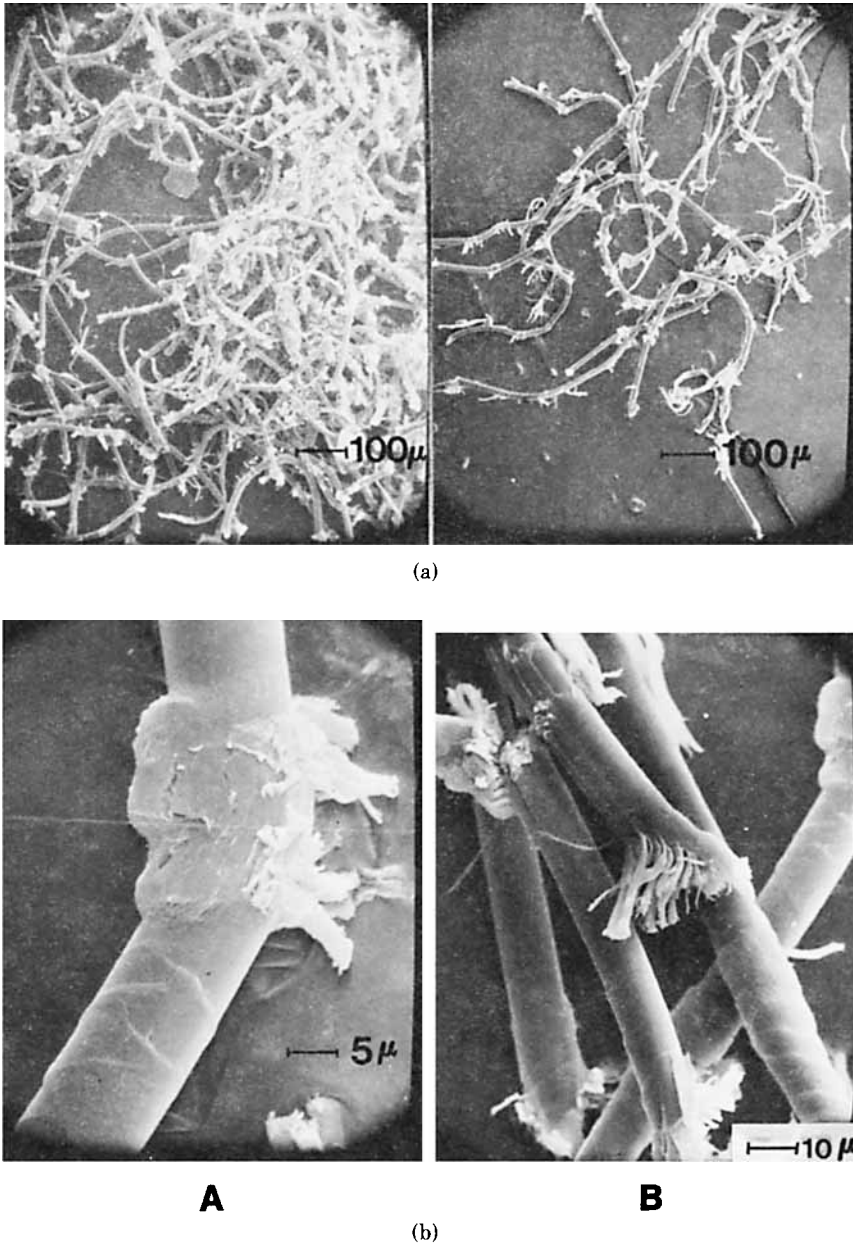


Fig. 8. (A) SEM photomicrographs of roll mill masticated Kevlar 29 (general view, and (B) SEM photomicrographs of roll mill masticated Kevlar 29: (a) point, (b) breakage.

value of about $100\ \mu\text{m}$, independent of the extent of flow. This kinking effect would appear to be owing to buckling induced by shear flow. We develop this view in the next section.

The problem is most difficult for the cellulose fibers. On the basis of photomicrographs (Figs. 4-7), we can evaluate only qualitatively that the changes of lengths for cellulose fibers are less significant than those for glass or aramid fibers.

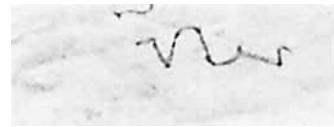
OPTICAL PHOTOMICROGRAPHS OF KEVLAR

AFTER PROCESSING

← 140 μ



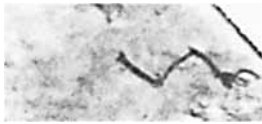
$$(A) \quad \bar{n} = 8; \quad \bar{L}_{tn} = 770\mu; \quad \frac{\bar{N}_w}{\bar{N}_n} = 1.4; \quad \frac{\bar{L}_{tw}}{\bar{L}_{tn}} = 1.4$$



$$(B) \quad \bar{n} = 6; \quad \bar{L}_{tn} = 580\mu; \quad \frac{\bar{N}_w}{\bar{N}_n} = 1.7; \quad \frac{\bar{L}_{tw}}{\bar{L}_{tn}} = 1.8$$



$$(C) \quad \bar{n} = 5; \quad \bar{L}_{tn} = 470\mu; \quad \frac{\bar{N}_w}{\bar{N}_n} = 1.6; \quad \frac{\bar{L}_{tw}}{\bar{L}_{tn}} = 1.6$$



$$(D) \quad \bar{n} = 4; \quad \bar{L}_{tn} = 380\mu; \quad \frac{\bar{N}_w}{\bar{N}_n} = 1.3; \quad \frac{\bar{L}_{tw}}{\bar{L}_{tn}} = 1.4$$

Fig. 9. Optical photomicrographs of Kevlar (after processing).

Mechanism of Breakage and Kinking of Fibers

Forgacs and Mason²⁷ have undertaken studies of particle motions and deformations of fibers of varying modulus and diameter. They observe rigid rotations, "springy" rotations with bending, and "snake" and "helix" rotations with considerable doubling up in elastomeric filaments. They also present an analysis for buckling. The forces which tend to bend and buckle a rotating fiber are the integral of the surface stresses along the length of the fiber.

$$F = - \int_{-L/2}^{+L/2} \pi d \sigma_s dl = \left(\frac{\pi d^2}{4} \right) \sigma_f \quad (4)$$

TABLE III
Glass Fiber Length Distribution (Sample Size of 100 Fibers)^a

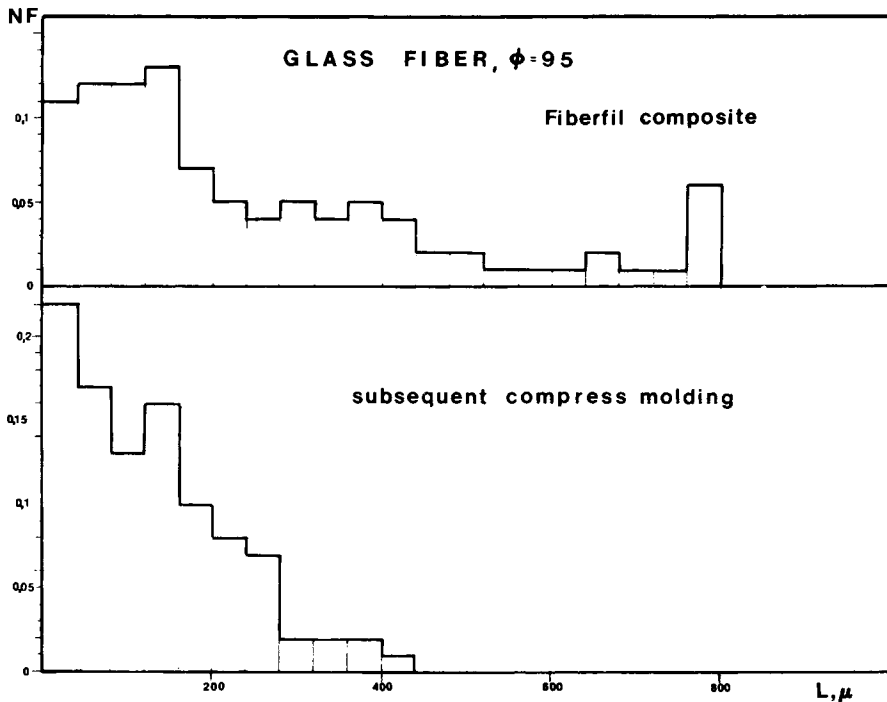
Sample	$\bar{L}_n, \mu\text{m}$	$\bar{L}_w, \mu\text{m}$	$\bar{L}_z, \mu\text{m}$	\bar{L}_w/\bar{L}_n
22 vol %				
As received	190	409	588	2.2
Compression molding, no mastication	105	178	226	1.7
30 min masticated	77	146	194	1.9
60 min masticated	51	117	160	2.3
9.5 vol %				
As received	210	530	707	2.5
Compression molding	112	190	303	1.7

$$^a \bar{L}_n = \frac{\sum n_i L_i}{\sum n_i}; \bar{L}_w = \frac{\sum n_i L_i^2}{\sum n_i L_i}; \bar{L}_z = \frac{\sum n_i L_i^3}{\sum n_i L_i^2}$$

It is these flow-induced stresses σ_f often in the bending mode which we believe damage and break fibers.

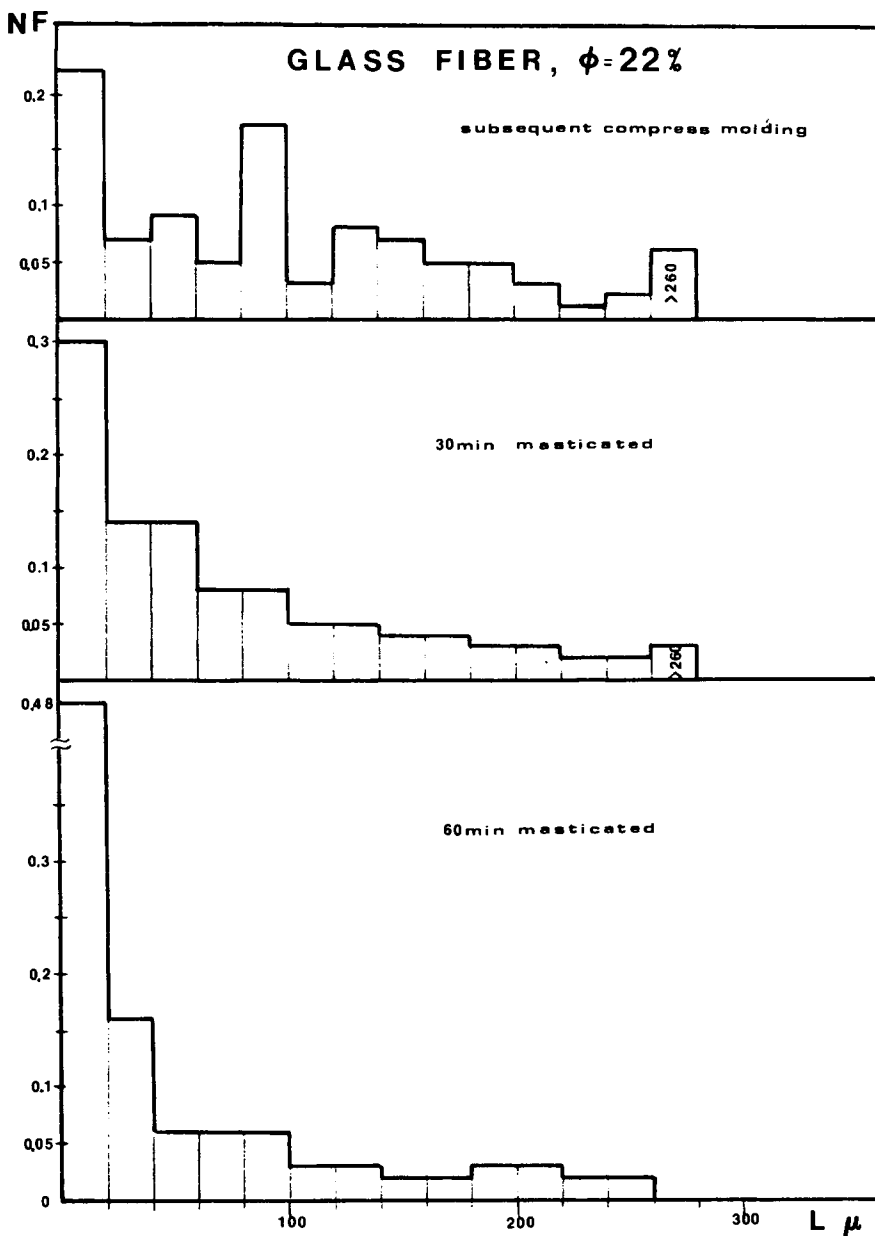
Forgacs and Mason²⁷ point out that for a rigid rod in shear flow in an infinitely dilute suspension, this stress is

$$F = \frac{\eta}{4} \frac{\pi L^2 M(\phi)}{\left[\ln \left(\frac{2L}{d} \right) - 1.75 \right]} \dot{\gamma} \quad (5)$$



(a)

Fig. 10. (a) Glass fiber length distribution for Fiberfil composite ($\phi = 9.5\%$) and for the subsequent compression molding. (b) Glass fiber length distribution for the compression molding composite ($\phi = 22\%$) and after 30 and 60 min mastication.



(b)


Fig. 10 (Continued from the previous page.)

where M is a factor which depends on orientation and reaches its maximum of $1/2$ in a plane shear flow at $\phi = 45^\circ$ to the direction of flow. This is of course an approximation because our systems are not dilute. If we presume the stress varies linearly along the length of the fiber, then, from eq. (4),

$$F_{\max}(\phi = 45^\circ) = \frac{1}{2}f_{\max}L^2 \tag{6a}$$

TABLE IV
Kevlar Fiber Length Distribution (Sample Size of 100 Fibers)^a

Quantity designator	0 min ^c		30 min		60 min		90 min		Remarks
	1270 μm ^c	635 μm	635 μm	635 μm	1270 μm	635 μm	635 μm	635 μm	
Total fiber length	\bar{L}_{tn} 735.0	612.0	580.0	486	473	382			
	\bar{L}_{tw} 998.0	1093	1004	764	762	522			
	\bar{L}_{tz} 1320	1502	1361	1232	1028	801			
Total fiber length dispersity	$\bar{L}_{tw}/\bar{L}_{tn}$ 1.4	1.8	1.8	1.6	1.6	1.4			
Number of segments in fiber	\bar{N}_n 7.70	6.3	6.1	5.1	4.7	3.9			
	\bar{N}_w 10.2	10.9	10.2	7.8	7.4	5.2			
	\bar{N}_z 13.0	14.6	13.5	12.2	9.7	7.8			
Segment dispersity	\bar{N}_w/\bar{N}_n 1.3	1.7	1.7	1.5	1.6	1.3			
Segment length	\bar{L}_{jn} 96.0	97.0	96.0	95.0	101.0	99.0			98 ± 2
	\bar{L}_{jw} 98.0	100.0	99.0	98.0	103.0	101.0			100 ± 2
	\bar{L}_{jz} 101.0	103.0	101.0	101.0	106.0	103.0			103 ± 2
Segment length dispersity	$\bar{L}_{jw}/\bar{L}_{jn}$ 1.02	1.03	1.03	1.03	1.02	1.02			1.02

; $N =$ number of segments in single fiber, $L_i = \sum_{i=1}^n L_{ji}$; $\bar{L}_n = \frac{\sum n_i L_i}{\sum n_i}$, $\bar{L}_w = \frac{\sum n_i L_i^2}{\sum n_i L_i}$, $\bar{L}_z = \frac{\sum n_i L_i^3}{\sum n_i L_i^2}$, $\bar{N}_n = \frac{\sum n_i N_i}{\sum n_i}$, $\bar{N}_w = \frac{\sum n_i N_i^2}{\sum n_i N_i}$, $\bar{N}_z = \frac{\sum n_i N_i^3}{\sum n_i N_i^2}$.

^b Mastication time.

^c Initial length.

where

$$f_{\max} = \frac{\eta}{4} \left[\frac{\pi}{\log\left(\frac{2L}{d}\right) - 1.75} \right] \dot{\gamma} \tag{6b}$$

and the compressive force at some position l is

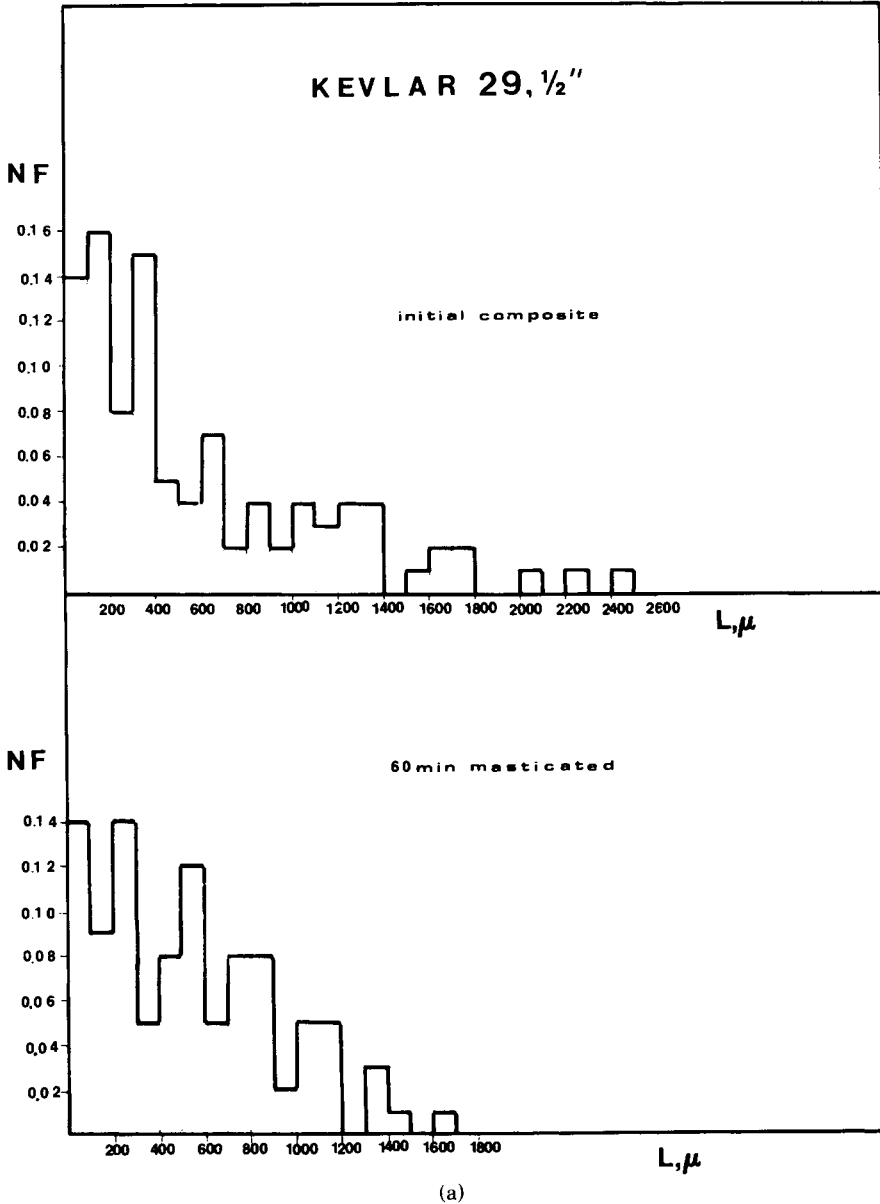
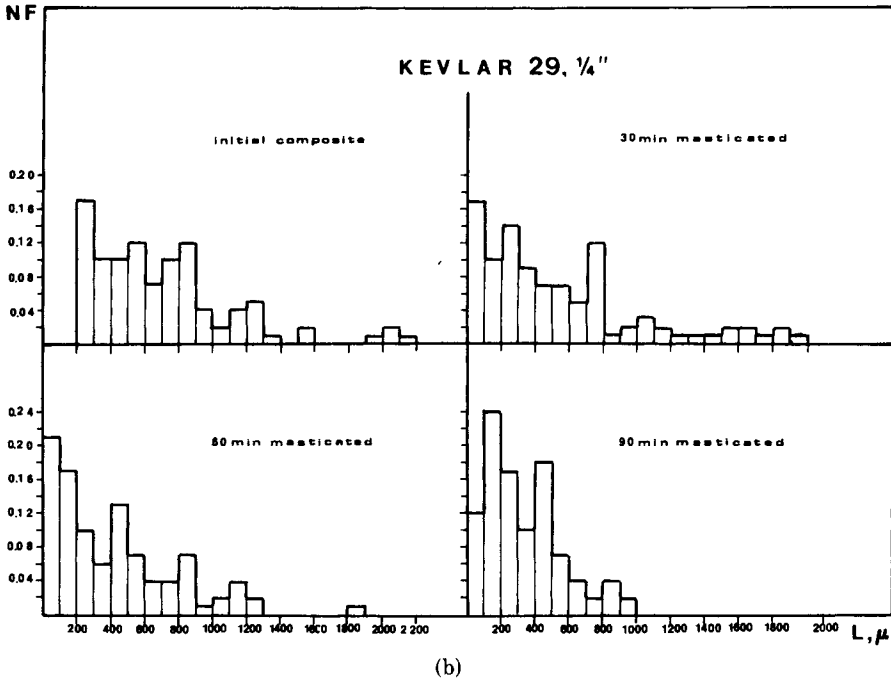


Fig. 11. (a) Kevlar fiber length distribution ($L_0 = 1/2$ in.) in initial composite and after 60 min mastication. (b) Kevlar fiber length distribution ($L_0 = 1/4$ in.) in initial composite and after 30, 60, and 90 min mastication.



(b)
Fig. 11 (Continued from the previous page.)

$$F(l) = \frac{f_{\max}(L^2 - l^2)}{2} \quad (7)$$

We now turn to the problem of buckling.²⁸ The equation for the shape $y(l)$ of a rod under compressive forces at its ends is

$$E_b I \frac{d^2 y}{dl^2} = -F(l)y \quad (8)$$

where E_b is the bending modulus. If we substitute eq. (7) into eq. (8), we may solve this equation for y , which has the dimensionless solution

$$\frac{y}{L} = \frac{y}{L} \left[\frac{F_{\max} L^2}{E_b I}, \frac{l}{L} \right] \quad (9a)$$

The modes of buckling occur when

$$\frac{F_{\max} L^2}{E_b I} \approx 2n + 1 \quad (9b)$$

By combining eqs. (6) and (9b), we may determine the shear rates required for buckling in a medium of viscosity η .

The bending stresses σ_b at points along the filament correspond to

$$\sigma_b \sim \sigma_f \sim \frac{F_{\max}}{\pi d^2/4} \sim \frac{4(2n+1)}{\pi} \frac{E_b I}{L^2 d^2} \sim \frac{2n+1}{16} E_b \left(\frac{d}{L} \right)^2 \quad (10)$$

Bending failure would be expected to occur at a critical value of σ_b , say Y . A critical value of L/d corresponding to 100/12 is clearly required for σ_b to reach Y for aramid fibers. For glass fibers, only, a very small L/d value is required. Cellulose fibers appear to be "prebuckled" as mentioned earlier.

For fibers of equivalent L/d and modulus, breakage would appear to depend

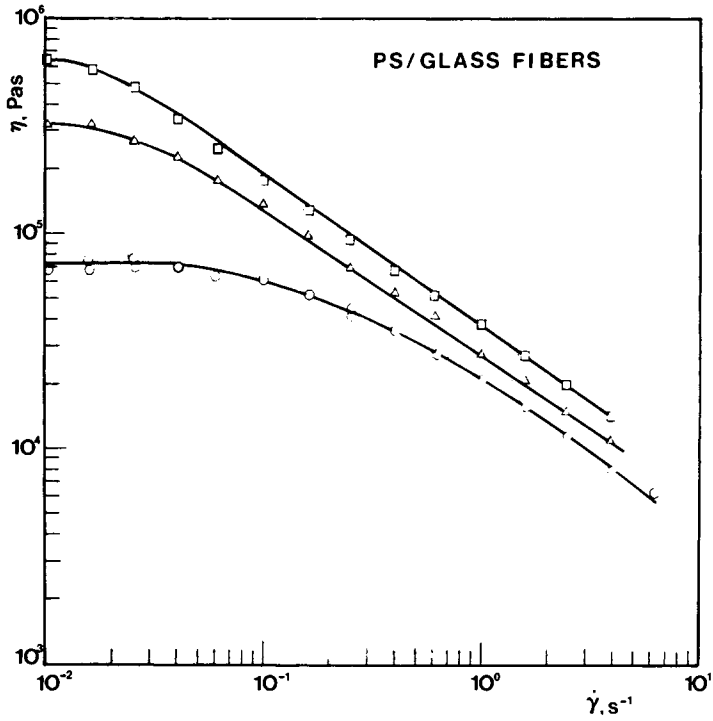


Fig. 12. Shear viscosity η as a function of shear rate ($\dot{\gamma}$) for the PS melt with 0 (O) 9.5 (\square) and 22 (Δ) vol % glass fibers, $T = 180^\circ\text{C}$.

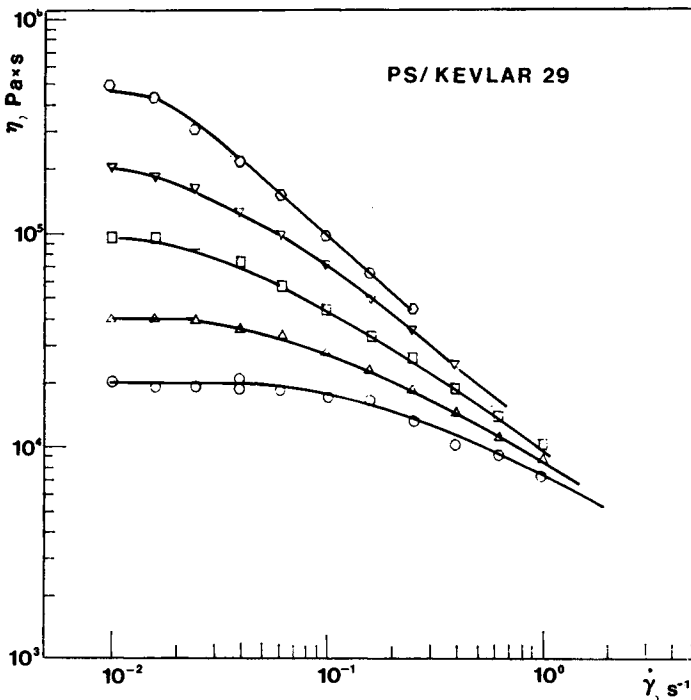


Fig. 13. Shear viscosity η as a function of shear rate $\dot{\gamma}$ for the PS melt with 0 (O), 1 (Δ), 5 (\square), 10 (∇), and 20 (\circ) vol % Kevlar fibers, $T = 180^\circ\text{C}$.

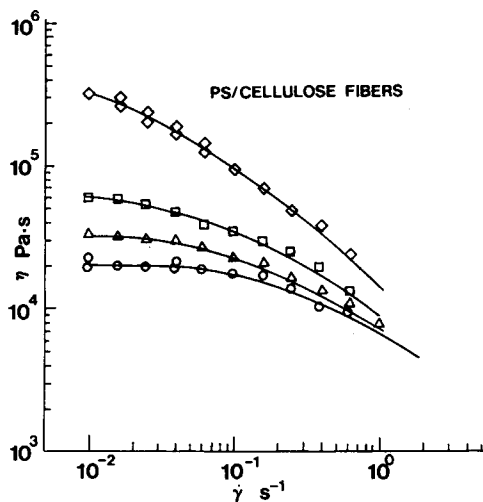


Fig. 14. Shear viscosity η as a function of shear rate $\dot{\gamma}$ for the PS melt with 0 (O), 1 (Δ), 5 (\square), and 20 (\diamond) vol % cellulose fibers, $T = 180^\circ\text{C}$.

on bending strength. This suggests using knot tests to order rates of fiber breakage under equivalent conditions. This of course leads to results equivalent to those observed here.

VISCOSITY

Results

Viscosity shear rate curves for the polystyrene melt with varying levels of glass, aramid, and cellulose fibers are shown in Figures 12 through 14. We see in all

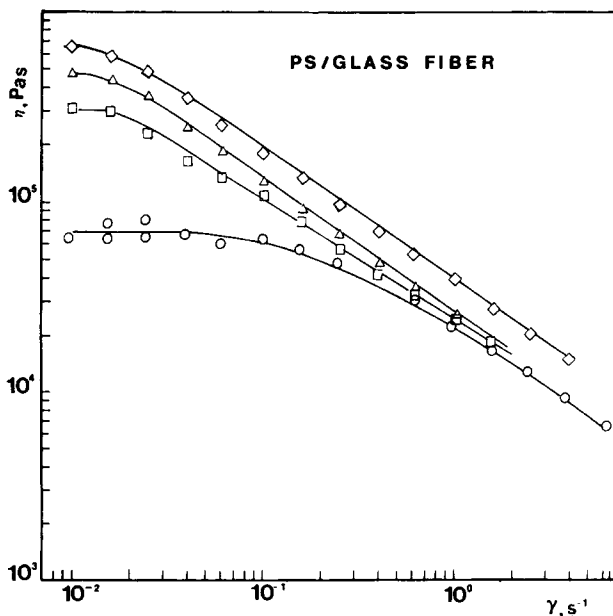


Fig. 15. Shear viscosity η as a function of shear rate $\dot{\gamma}$ for the PS melt with 0 and 22 vol % glass fibers before mastication and after 30 and 60 min mastication, $T = 180^\circ\text{C}$.

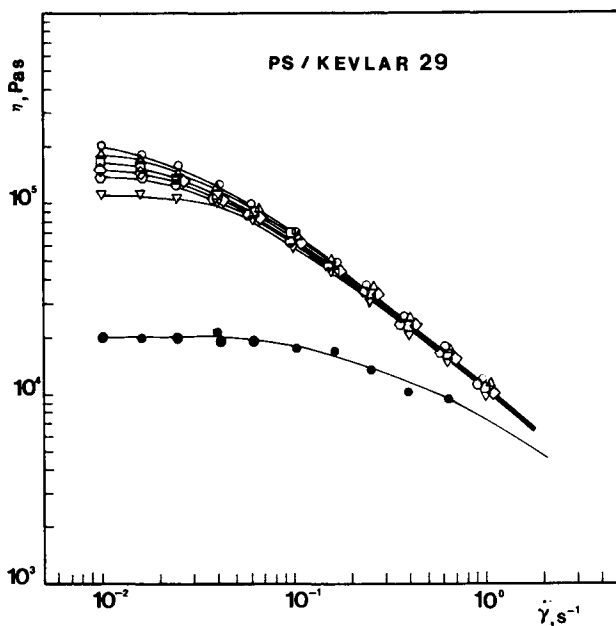


Fig. 16. Shear viscosity η as a function of shear rate $\dot{\gamma}$ for the PS melt with 0 and 10 vol % Kevlar fibers ($L_0 = 1270$ and $635 \mu\text{m}$) before mastication and after 30, 60, and 90 min mastication, $T = 180^\circ\text{C}$.

cases that the viscosity is increased by the presence of the fibers and is constant at low shear rates and decreases with increasing shear rate. The glass fiber systems studied are the same as those of Chan et al.,⁴ and our results agree with theirs. The data on Kevlar and cellulose fibers are new.

The influence of extensive mastication of glass- and aramid-fiber-reinforced polystyrene is shown in Figures 15 and 16. Generally, extent of mastication reduces the viscosity in both systems. The greatest effect is in the glass-fiber-reinforced melts.

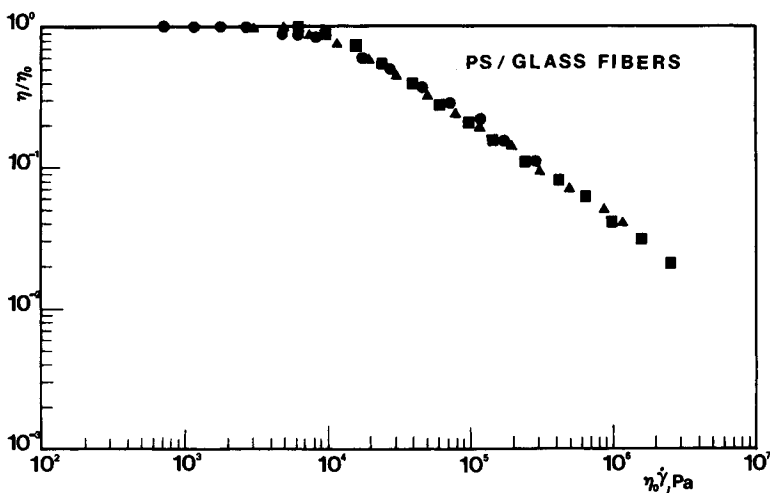


Fig. 17. Master curve η/η_0 vs. $\eta_0\dot{\gamma}$ for the PS melt with 0 (●), 9.5 (▲), and 22 (■) vol % glass fibers.

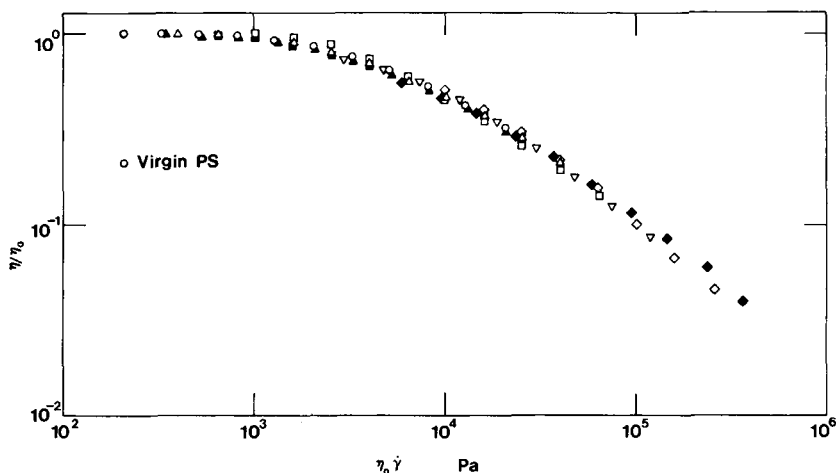


Fig. 18. Master curve η/η_0 vs. $\eta_0\dot{\gamma}$ for the PS melt with 0 (O), 1 (\blacktriangle), 5 (\blacksquare), and 20 (\blacklozenge) vol % cellulose fibers and 0 (O), 1 (\triangle), 5 (\square), 10 (∇), and 20 (\diamond) Kevlar fibers.

Discussion

We shall attempt in this section to interpret the viscosity η -shear rate $\dot{\gamma}$ behavior of fiber-reinforced polymer melts. It is useful to begin by briefly considering the characteristics of the viscosity-shear rate behavior. The behavior of the polystyrene melt shown in Figures 12 through 14 is typical, with the viscosity a constant, η_0 , at low shear rates and then decreasing at higher shear rate. Vinogradov and Malkin²⁹ have proposed that viscosity-shear rate data can be correlated in a reduced form by plotting $\eta(\dot{\gamma})/\eta_0$ vs. $\eta_0\dot{\gamma}$:

$$\eta(\dot{\gamma}) = \eta_0 F[\eta_0\dot{\gamma}] \quad (11)$$

Similar plots have been proposed by other investigators such as Sabia³⁰ and

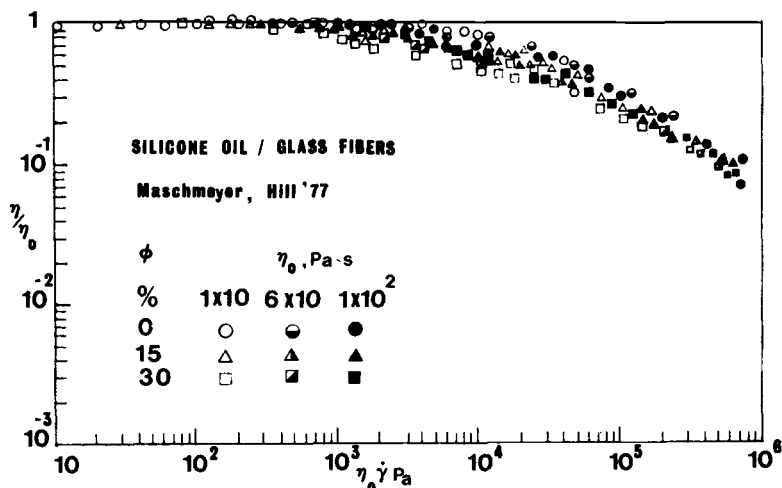


Fig. 19. Master curve η/η_0 vs. $\eta_0\dot{\gamma}$ for the silicone oil ($\eta_0 = 10, 60,$ and $100 \text{ Pa}\cdot\text{s}$) with 0, 15, and 30 vol % glass fibers. After Maschmeyer and Hill.³²

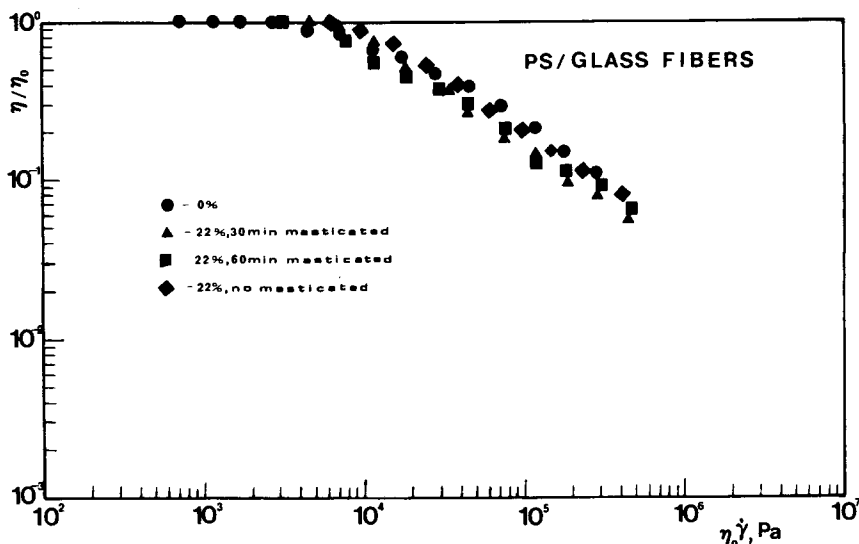


Fig. 20. Master curve η/η_0 vs. $\eta_0\dot{\gamma}$ for the PS melt with 0 and 22 vol % glass fibers before mastication and after 30 and 60 min mastication.

Graessley.^{31,32} They use a $\tau_0\dot{\gamma}$ in which τ_0 is a characteristic time taken, for example, as a reciprocal of the shear rate at which the viscosity function becomes non-Newtonian. Generally, plots of η/η_0 vs. $\eta_0\dot{\gamma}$ or $\tau_0\dot{\gamma}$ are temperature independent but depend upon molecular weight distribution, with η/η_0 decreasing more rapidly with increasing shear rate in broad distribution systems.^{32,35}

In Figures 17 and 18 we plot the reduced viscosity η^*/η_0^* (suspension) and η/η_0 (pure melt) vs. $\eta_0^*\dot{\gamma}$ (and $\eta_0\dot{\gamma}$) for the suspensions of glass, aramid, and cellulose fibers whose raw data are shown in Figures 12 through 14. The overlap is seen to be very good, indicating that eq. (11) is obeyed. It is also possible to make comparisons with other data in the literature. In Figure 19 we plot the data of Maschmeyer and Hill⁷ on glass fibers in a slightly non-Newtonian oil. Again the data satisfy eq. (11).

In Figures 20 and 21 we plot η/η_0 vs. $\eta_0\dot{\gamma}$ for the masticated glass- and aramid-fiber-reinforced melts. Again superposition is obtained.

The addition of fibers to a polymer melt acts in its influence on viscosity like a reduction in temperature in the melt. This supports the idea that the enhanced viscosity is due to increased viscous dissipation in the matrix and that particle-particle interaction is not significant.

Suspension Mechanics Interpretation

We attempt in this section to justify eq. (11) based upon the mechanics of suspensions. In suspensions with noninteracting particles, the viscosity is enhanced by the increased energy dissipation owing to the presence of the solid particles. The theory of this viscosity enhancement in a suspension owing to enhanced energy dissipation is due to Einstein³⁶ (cf. Batchelor³⁷) who considered the case of a dilute suspension of spheres. This has since been extended to more concentrated systems and to particles with other shapes. Reviews are given by

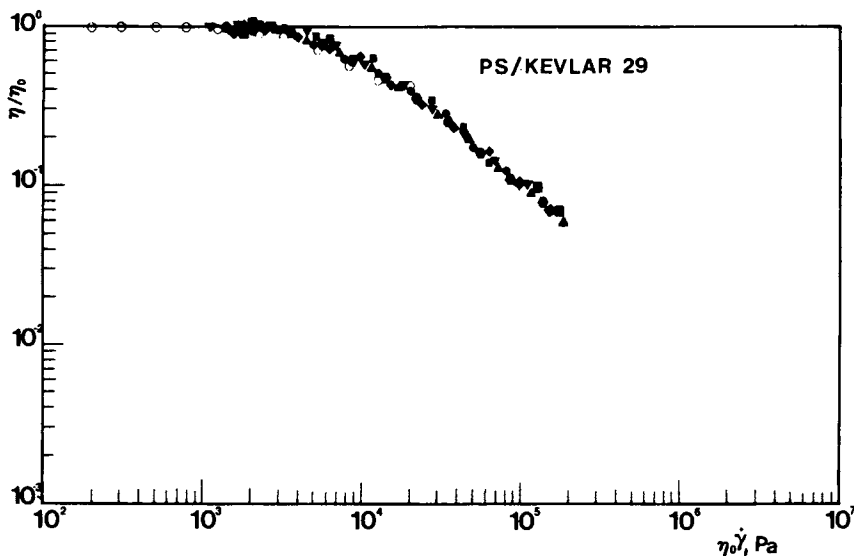


Fig. 21. Master curve η/η_0 vs. $\eta_0\dot{\gamma}$ for the PS melt with 0 and 10 vol % Kevlar fibers before mastication and after 30, 60, and 90 min mastication.

Happel and Brenner³⁸ and Jeffrey and Acrivos,³⁹ among others. The viscosity η^* of a suspension of particles in shear flow can be expressed in the absence of interparticle force fields is given by

$$E = \eta^* \dot{\gamma}^2 V = \int \sigma : \nabla \mathbf{v}_s dV \quad (12)$$

where E is the energy dissipated within the apparatus and subscript s refers to the matrix fluid without suspended particles.

Theories of the shear viscosity of concentrated suspensions have been based generally upon cell models of concentrated suspensions as developed by Simha⁴⁰ and Happel.⁴¹ In these theories the creeping flow Navier–Stokes equations were solved for a matrix of spheres in arbitrarily defined cells and the boundary conditions matched. The viscosity is computed from eq. (14). A striking innovation in concentrated suspension mechanics was made by Frankel and Acrivos,⁴² who showed that one could simply use the Reynolds lubrication theory⁴³ to evaluate the dissipation of energy between particles. A second application of lubrication theory to suspension mechanics was devised by Batchelor,⁴⁴ who considered the case of elongational flow of fiber-reinforced fluid. The parallelism of the fibers allows one to represent the stress field and energy dissipation in terms of viscous shearing action and lubrication theory.

The simplicity of lubrication theory suggests that one may extend the concepts of suspension mechanics to non-Newtonian matrix systems. This was first carried out by Goddard^{45,46} for the case of elongational flow of a concentrated suspension of fibers. It is clearly very difficult to apply such arguments to the shear flow of suspensions of fibers in a viscoelastic fluid such as a polymer melt. Indeed, in any lubrication argument based on an approach such as Frankel and Acrivos,⁴² we must be concerned with the effect of viscoelastic phenomena in squeeze films. Putting that problem aside, it should be clear that application

of a lubrication-type argument with the stress tensor determined by a shear viscosity only will lead in to an increased shear viscosity of form

$$\sigma_{12} = \eta^*(\dot{\gamma})\dot{\gamma} = \eta_s(I_1\dot{\gamma})I_2\dot{\gamma} \quad \eta_0^* = I_2\eta_{s0} \quad (13)$$

where I_1 and I_2 are numerical factors greater than unity, which account for the increased rate of shearing between the particles; and $I_2\dot{\gamma}$ represents the average shear rate between the particles. The quantities I_1 and I_2 are larger than unity but should be similar in magnitude. If the viscosity of the suspending medium η_s obeys eq. (11), it follows that

$$\eta^*(\dot{\gamma}) = I_2\eta_{s0}F[I_1\eta_0\dot{\gamma}] \quad (14)$$

This suggests the form

$$\eta^*(\dot{\gamma}) = \eta_0^*F\left[\frac{I_1}{I_2}\eta_0^*\dot{\gamma}\right] \quad (15a)$$

or with I_1 equal to I_2

$$\eta^*(\dot{\gamma}) = \eta_0^*F[\eta_0^*\dot{\gamma}] \quad (15b)$$

where η_0^* is the zero shear viscosity of the suspension. Equation (15b), of course, rigorously depends on I_1 being equal to I_2 . Equation (15b) indicates that a plot of $\eta^*(\dot{\gamma})/\eta_0^*$ vs. $\eta_0^*\dot{\gamma}$ should be of the same form as for the virgin melt, which is what we observe.

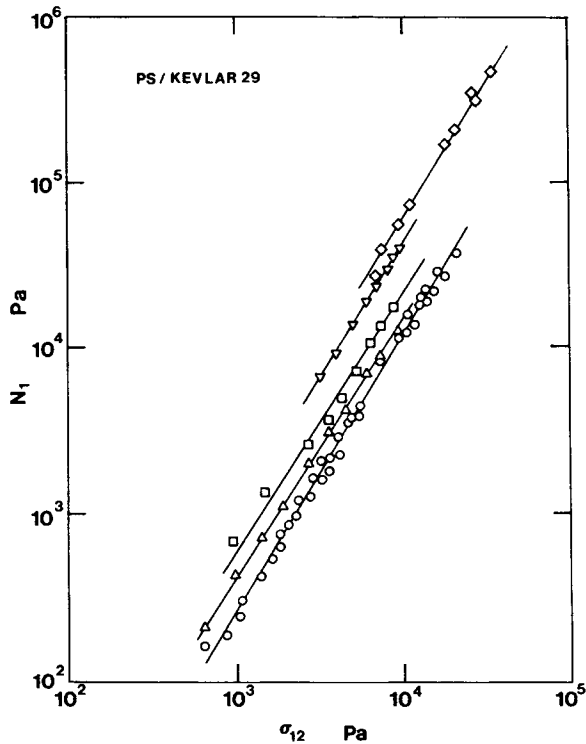


Fig. 22. Principal normal stress difference N_i as function of shear stress σ_{12} for the PS melt with 0 (O), 1 (Δ), 5 (\square), 10 (∇) and 20 (\diamond) vol % Kevlar fibers.

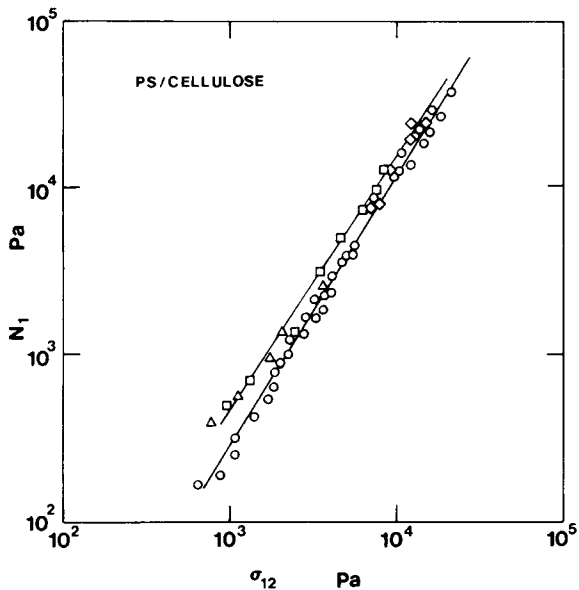


Fig. 23. Principal normal stress difference N_1 as function of shear stress σ_{12} for the PS melt with 0 (O), 1 (Δ), 5 (\square), and 20 (\diamond) vol % cellulose fibers.

PRINCIPAL NORMAL STRESS DIFFERENCE

Results

We plot the principal normal stress difference N_1 for the glass-, aramid-, and cellulose-fiber-reinforced polymer melts in Figures 22 through 24 as a function of shear stress σ_{12} . It may be seen that N_1 increases with both shear rate and shear stress.

The glass fiber systems are again the same as those studied by Chan et al.⁴ The values of N_1 we have obtained are somewhat higher than those of these authors.

The effects of mastication on principal normal stress difference for the glass and Kevlar systems are seen in Figures 25 and 26. Clearly, mastication reduces N_1 more rapidly than σ_{12} .

Interpretation

The correlations between N_1 and σ_{12} are of great interest because they show the *relative* influence of the fibers on the principal normal stress difference and the shear stress and not the influence of N_1 alone. They are also of interest from the studies of Oda, White, and Clark⁴⁸ and Minoshima et al.³⁵ (see also Han⁴⁹), who note for pure melts the N_1 - σ_{12} independence of temperature and apparently (flexible) polymer chain backbone but dependence upon molecular weight distribution. It is seen that N_1 is increased by fibers to a greater extent than σ_{12} .

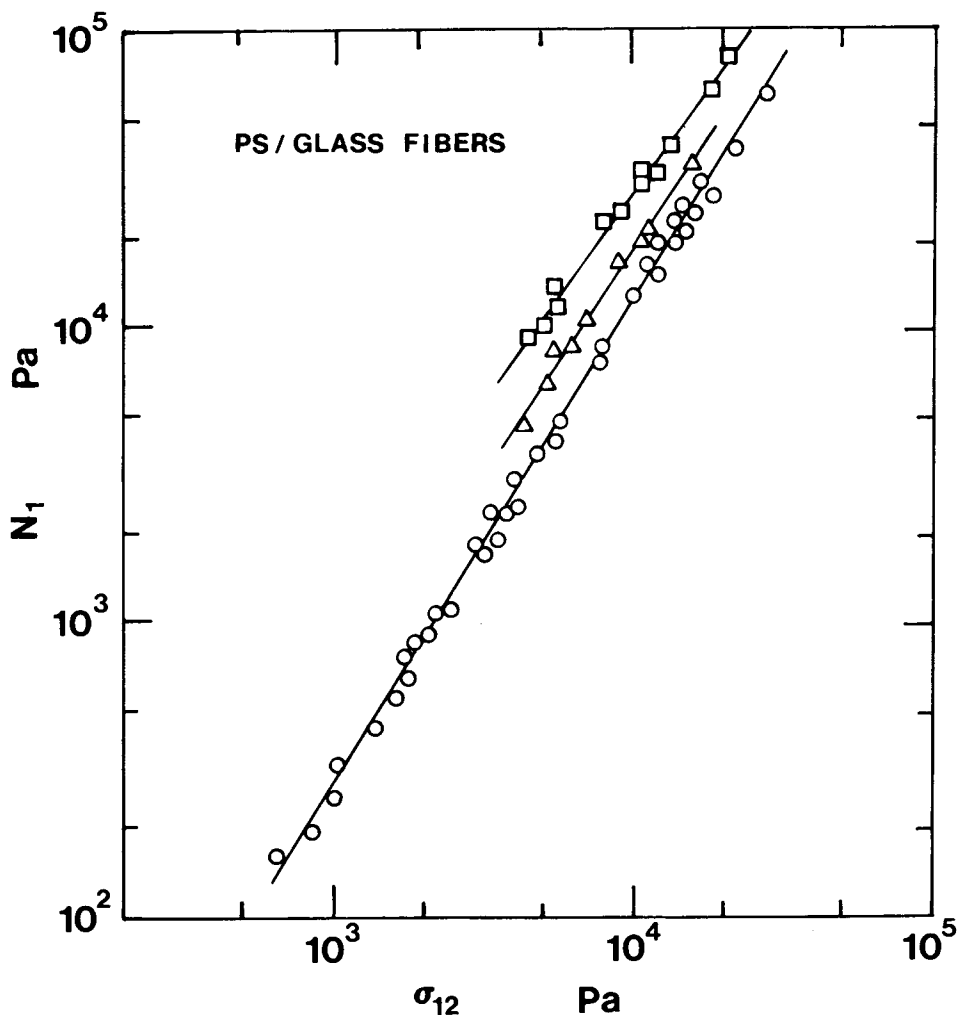


Fig. 24. Principal normal stress difference N_1 as function of shear stress σ_{12} for the PS melt with 0 (O), 10 (Δ), and 22 (\square) vol % glass fibers.

The influence of fibers on the N_1 - σ_{12} relationship is different from that for small particles. Studies in our own laboratory for carbon black- and titanium dioxide-reinforced polymer melts indicate that N_1 is decreased by the presence of particles.¹⁸⁻²⁰ Similar results are obtained by Han⁵⁰ for a calcium carbonate-reinforced polypropylene.

The mechanism for the large normal stresses in fiber-reinforced melts is presumably that given by Chan et al.⁹ It is due to normal stresses being caused not only by the continuous medium but also by particle effects, as indicated by the Weissenberg rod climbing effects found in suspensions of fibers in Newtonian fluids.⁵¹⁻⁵³

The reduction in N_1 at fixed σ_{12} for the masticated fiber-reinforced melts (Figs. 25 and 26) is clearly due to the breakdown of the fibers.

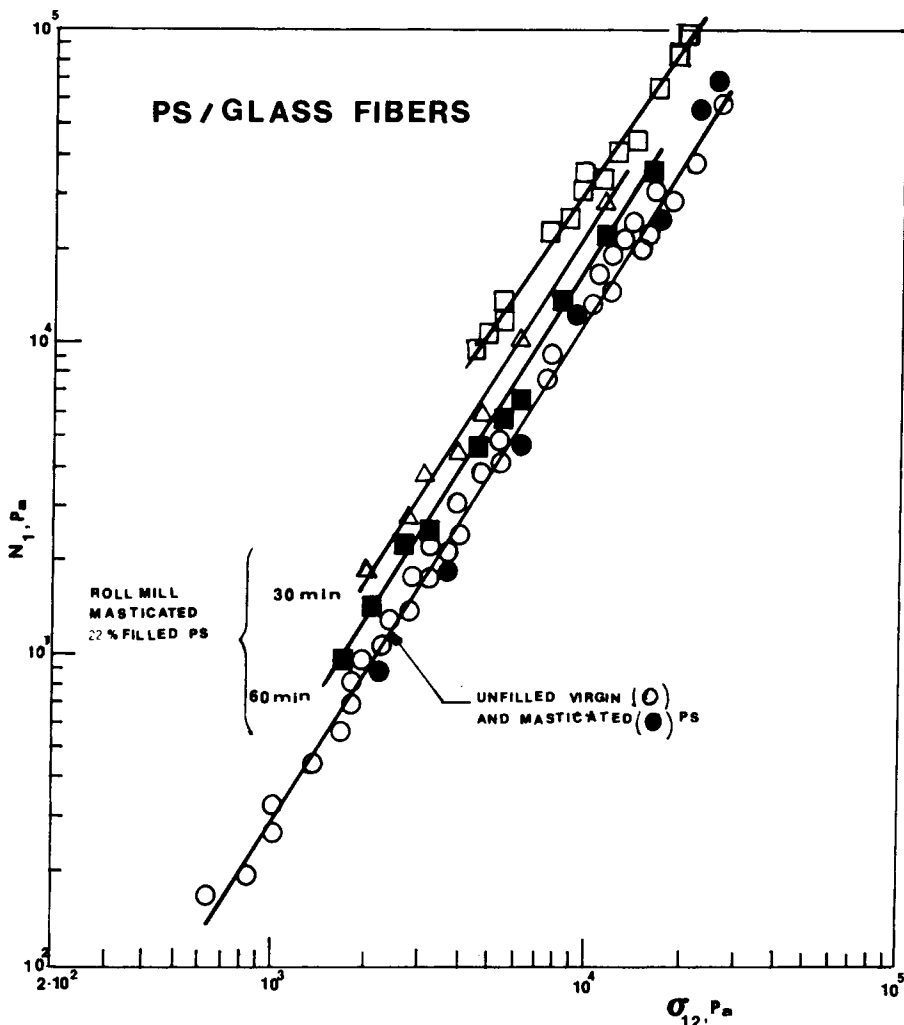


Fig. 25. Principal normal stress difference N_1 as function of shear stress σ_{12} for the PS melt with 0 and 22 vol % glass fibers before mastication and after 30 and 60 min mastication.

Oda, White, and Clark⁴⁸ and Minoshima et al.³⁵ represented their data on homogeneous melts through the expression

$$N_1 = A\sigma_{12}^a \quad (16)$$

and related the parameters A and a to molecular weight distribution. The parameter A corresponds roughly to the steady-state compliance J_e . We may similarly relate A in fiber-filled melts to the fiber loading and aspect ratio. These parameters are listed for the different systems studied in Table V. The value of exponent a does not change. We plot A as a function of volume loading and aspect ratio of fibers in Figures 27 and 28 for glass and Kevlar. It is evident that

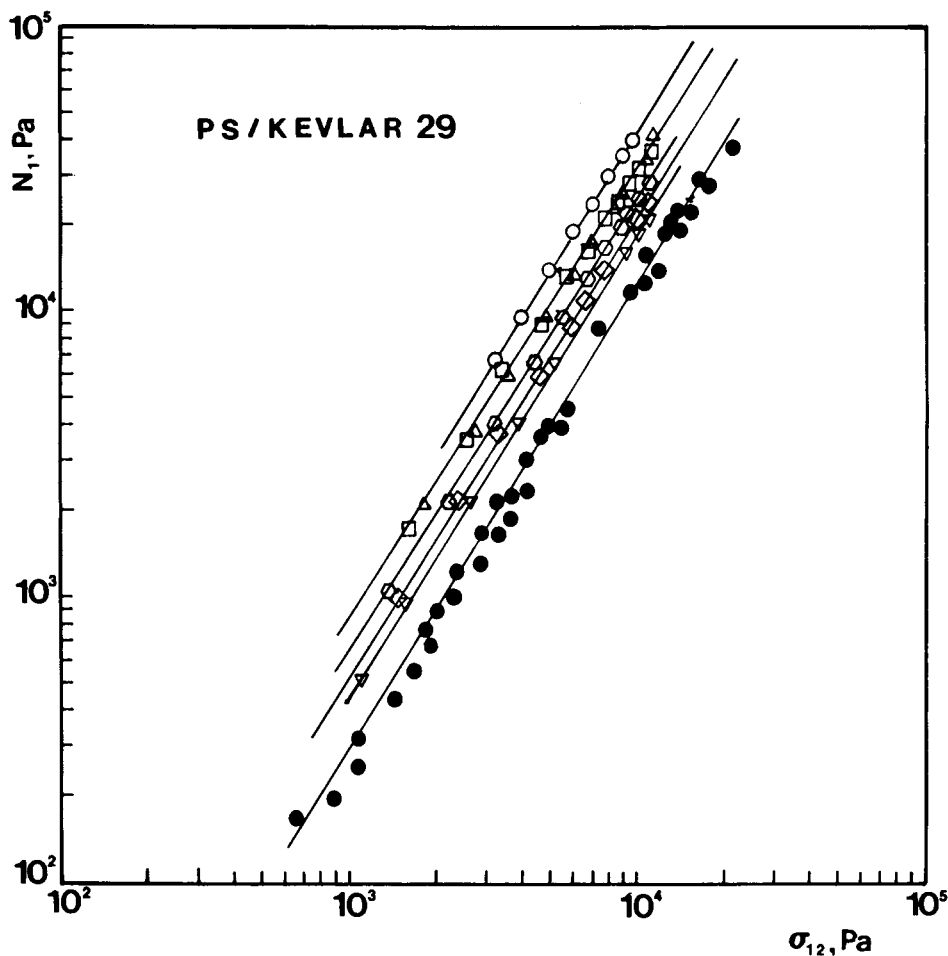


Fig. 26. Principal normal stress difference N_1 as a function of shear stress σ_{12} for the PS melt with 0 and 10 vol % Kevlar fibers ($L_0 = 1270$ and $635 \mu\text{m}$) before mastication and after 30, 60, and 90 min mastication.

A is an increasing function of both parameters, but the functionality differs for the fibers. The values of A are larger for Kevlar. Clearly, it depends on volume fraction, aspect ratio, and fiber modulus:

$$A = A(\phi, L/D, E) \tag{17}$$

The influence of the partial breakage of the Kevlar fibers is not clear.

COMPARATIVE ASSESSMENT OF FIBER DAMAGE EFFECTS ON RHEOLOGICAL PROPERTIES

It is useful to conclude by summarizing our results on the different fiber systems investigated:

TABLE V
Values of Oda-White-Clark A and α Parameters for Fiber-Reinforced Polystyrene

Fiber	ϕ , %	L/D	$A \times 10^{-3}$	α^a
Glass	0		3.2	1.64
	9.5	8.8	4.7	1.65
	22.0	8.3	6.8	1.66
	22.0	6.7	6.0	1.65
	22.0	4.3	4.6	1.64
	1.0	60.3	7.2	1.58
	5.0	60.3	11.0	1.58
	10.0	60.3	14.0	1.63
	10.0	50.2	13.0	1.60
	10.0	47.5	13.0	1.60
	10.0	33.9	7.6	1.61
	10.0	38.8	7.8	1.61
	10.0	31.3	3.7	1.68
	20.0	60.3	16.0	1.65
Cellulose	20.0	~ 100	5.9	1.62

^a $\bar{\alpha} = 1.63 \pm 0.3$.

(1) Fibers may be damaged during mixing into polymer melts or from subsequent mastication during processing. The character and extent of damage vary with polymer type and are more severe for the glass fibers. The aramid (Kevlar 29) break down but often without clean breaks, possessing kinks separated by distances of 100 μm . The cellulose fibers show the least damage in

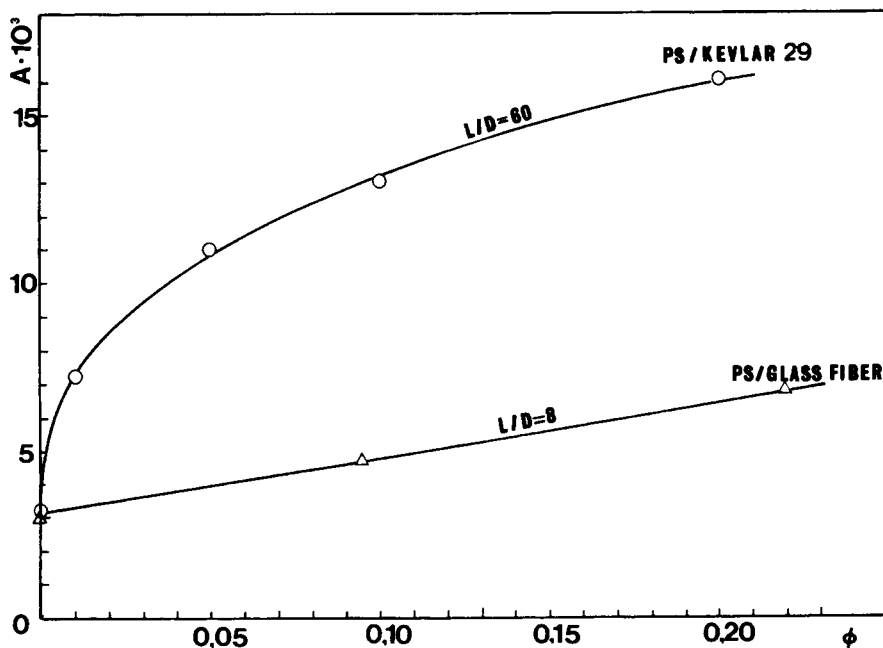


Fig. 27. The Oda-White-Clark equation factor A as function of fiber loading level Φ for the PS melt with glass and Kevlar fibers.

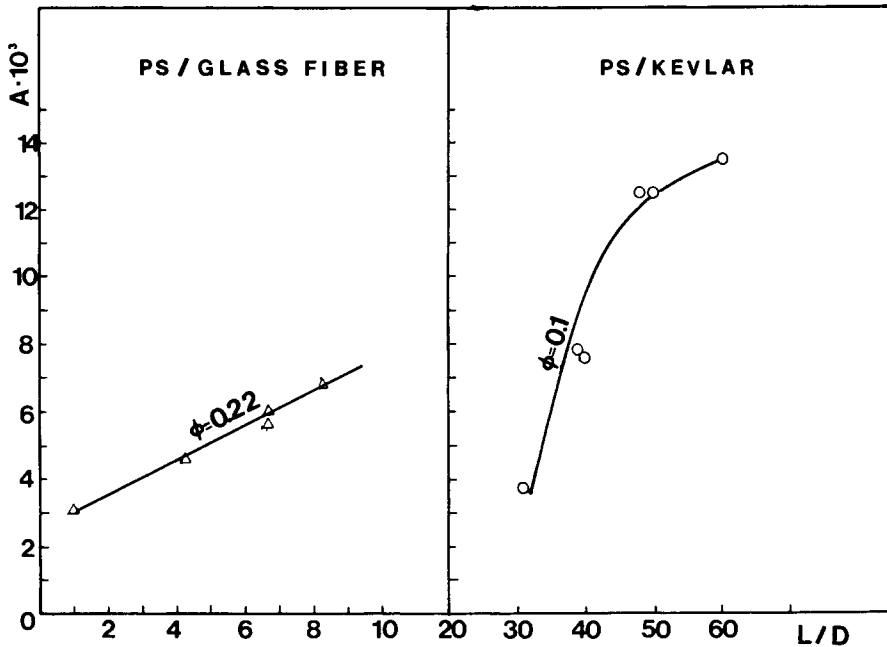


Fig. 28. The Oda-White-Clark equation factor A as function of fiber aspect ratio $4D$ for the PS melt with glass and Kevlar fibers.

processing. A theory of damage based on failure induced by buckling that occurs in shear flow is described.

(2) Addition of aramid, cellulose, and glass fibers with diameters of $12 \mu\text{m}$ to polymer melts results in an increase in viscosity but does not change the basic character of the viscosity shear rate behavior of the polymer melts studies. Indeed, the suspensions continue to follow the Vinogradov-Malkin superposition curve, showing that addition of fibers has an effect equivalent to lowering the temperature. This would seem to indicate that the viscosity rise is due solely to hydrodynamic factors and not to interparticle forces.

(3) Addition of fibers causes the principal normal stress difference N_1 to be increased more rapidly than shear stress. This appears to be a hydrodynamic particle phenomenon as Weissenberg effects have been observed in Newtonian fluid suspensions of fibers. N_1 increases with fiber aspect ratio and modulus and is lower for masticated systems containing damaged fibers and for the cellulose fibers.

This research was supported in part by the National Science Foundation under NSF Grant ENG 76-19815. The authors gratefully acknowledge this support. They would like to especially thank B. L. McGill for his help in obtaining the SEM photomicrographs. We thank Mr. W. Minoshime for his help in the preparation of figures.

References

1. J. C. Halpin and N. J. Pagano, *J. Compos. Mater.*, **3**, 720 (1969).
2. H. Brody and I. M. Ward, *Polym. Eng. Sci.*, **11**, 139 (1971).
3. W. Zielinski, *Polimery*, **18**, 170 (1973).

4. L. Zakrzewski, *Przem. Chem.*, **52**, 150 (1973).
5. Z. Kohman, *Polimery*, **20**, 27 and 74 (1975).
6. A. Y. Coran, P. Hamed, and L. A. Goettler, *Rubber Chem. Technol.*, **44**, 1167 (1976).
7. J. M. Charrier and J. M. Rieger, *Fibre Sci. Technol.*, **7**, 161 (1974).
8. Y. Oyanagi and Y. Yamaguchi, *J. Soc. Rheol. Jpn.*, **3**, 64 (1975).
9. Y. Chan, J. L. White, and Y. Oyanagi, *J. Rheol.*, **22**, 507 (1978); *Polym. Eng. Sci.*, **18**, 268 (1978).
10. S. Wu, *Polym. Eng. Sci.*, **19**, 638 (1979).
11. J. E. O'Connor, *Rubber Chem. Technol.*, **50**, 445 (1977).
12. R. O. Maschmeyer and C. T. Hill, *Trans. Soc. Rheol.*, **21**, 195 (1977).
13. L. A. Goettler, *Mod. Plast.*, 140 (April 1970); 20th Annual Technical Conference, Reinforced Plastics/Composition Division, Society of Plastics Industry, Section 14A, 1970, p. 1.
14. L. A. Goettler and A. J. Lambright, U.S. Pats. 4,056,591 (1977) and 4,057,610 (1977).
15. S. R. Moghe, *Rubber Chem. Technol.*, **45**, 1160 (1976).
16. J. L. White and J. W. Crowder, *J. Appl. Polym. Sci.*, **18**, 1013 (1974).
17. N. Minagawa and J. L. White, *J. Appl. Polym. Sci.*, **20**, 501 (1976).
18. V. M. Lobe and J. L. White, *Polym. Eng. Sci.*, **19**, 617 (1979).
19. J. L. White, *J. Non-Newt. Fluid Mech.*, **5**, 177 (1979).
20. H. Tanaka and J. L. White, *Polym. Eng. Sci.*, to appear.
21. H. S. Katz and J. V. Milewski, *Handbooks of Fillers and Reinforcements for Plastics*, Reinhold, New York, 1978.
22. K. Walters, *Rheometry*, Chapman and Hill, London, 1975.
23. W. E. Morton and J. W. S. Hearle, *Physical Properties of Textile Fibers*, 2nd ed., Wiley, New York, 1975.
24. C. C. Cheng, J. L. Cowart, B. L. McGill, J. E. Spruiell, and J. L. White, *Text. Res. J.*, **45**, 414 (1975).
25. H. Morawetz, *Macromolecules in Solution*, 2nd ed., Interscience, New York, 1975.
26. L. Konopasek and J. W. S. Hearle, *J. Appl. Polym. Sci.*, **21**, 2791 (1977).
27. O. L. Forgacs and S. G. Mason, *J. Colloid Sci.*, **14**, 457 (1959).
28. A. E. H. Love, *A Treatise on the Mathematical Theory of Elasticity*, 4th ed., Cambridge University Press, Cambridge, 1927.
29. G. V. Vinogradov and A. Y. Malkin, *J. Polym. Sci. Part B*, **2**, 671 (1964).
30. R. Sabia, *J. Appl. Polym. Sci.*, **7**, 347 (1963).
31. W. W. Graessley, *J. Chem. Phys.*, **47**, 1942 (1967).
32. W. W. Graessley and L. Segal, *Macromolecules*, **2**, 49 (1969).
33. N. Nishida, D. G. Salladay, and J. L. White, *J. Appl. Polym. Sci.*, **15**, 1181 (1971).
34. J. A. Cote and M. Shida, *J. Appl. Polym. Sci.*, **17**, 1639 (1973).
35. W. Minoshima, J. L. White, and J. E. Spruiell, *Polym. Eng. Sci.*, to appear.
36. A. Einstein, *Ann. Physik*, **19**, 289 (1906); **34**, 591 (1911).
37. G. K. Batchelor, *An Introduction to Fluid Dynamics*, Cambridge, London, 1967.
38. J. Happel and H. Brenner, *Low Reynolds Number Hydrodynamics*, Prentice-Hall, Englewood Cliffs, NJ, 1965.
39. D. J. Jeffrey and A. Acrivos, *AIChE J.*, **22**, 417 (1976).
40. R. Simha, *J. Appl. Phys.*, **23**, 1020 (1952).
41. J. Happel, *J. Appl. Phys.*, **27**, 1288 (1957).
42. N. A. Frankel and A. Acrivos, *Chem. Eng. Sci.*, **22**, 847 (1967).
43. O. Reynolds, *Philos. Trans. R. Soc. London*, **177**, 157 (1886).
44. G. K. Batchelor, *J. Fluid Mech.*, **46**, 813 (1971).
45. J. D. Goddard, *J. Non-Newt. Fluid Mech.*, **1**, 1 (1976).
46. J. D. Goddard, *J. Fluid Mech.*, **78**, 177 (1976).
47. G. Brindley, J. M. Davies, and K. Walters, *J. Non-Newt. Fluid Mech.*, **1**, 19 (1976).
48. K. Oda, J. L. White, and E. S. Clark, *Polym. Eng. Sci.*, **18**, 25 (1978).
49. C. D. Han, *Rheology in Polymer Processing*, Academic, New York, 1976.
50. C. D. Han, *J. Appl. Polym. Sci.*, **18**, 821 (1974).
51. M. A. Nawab and S. G. Mason, *J. Phys. Chem.*, **62**, 1248 (1958).
52. J. Mewis and A. B. Metzner, *J. Fluid Mech.*, **62**, 593 (1974).
53. R. O. Maschmeyer and C. T. Hill, *Adv. Chem. Ser.*, **134**, 95 (1974).

Received August 27, 1979